2007 IEEE International Conference on
Robotics and Automation
Roma, Italy, 10-14 April 2007

Robotic Electrolocation: Active Underwater Target Localization with Electric Fields

James R. Solberg Kevin M. Lynch Malcolm A. MacIver

Abstract— **We explore the capabilities of a robot designed to locate objects underwater through active movement of an electric field emitter and sensor apparatus. The robot is inspired by the biological phenomenon of active electrolocation, a sensing strategy found in two groups of freshwater fishes known to emit weak electric fields for target localization and communication. We characterize the performance of the robot using several types of automatic electrolocation controllers, objects, and water conditions. We demonstrate successful electrolocation both in the conditions in which it is naturally observed, in low conductivity water, as well as in conditions in which it is not observed, in water of ocean salinity. The belief of the position of the target is maintained via a particle filter and refined with each measurement.**

I. Introduction

The ability of some aquatic animals to sense electric fields was discovered in the late 1950s [8] and is therefore one of the most recently discovered biological sensing mechanisms. Many fish, such as sharks, sturgeons, and catfish, and some other animals, such as the platypus, are able to sense weak bioelectric fields emitted by aquatic prey and use these fields to locate prey. This ability is termed "passive electrolocation." Only two groups of freshwater fishes, one in South America and one in Africa, both emit and sense an electric field, similar to active sensing systems such as radar and sonar [15]. They are therefore referred to as active electrolocators. These fish utilize their self-generated weak electric field ($\sim$1 mV/cm near the body) to detect and identify objects in their environment—irrespective of whether these objects emit a bioelectric field as needed by passive electrolocators.

Active electrolocators hunt in total darkness and in cluttered and turbid environments where vision is useless [3], [23], [11]. The neural mechanisms of active electrolocation have become the subject of intense investigation, making "weakly electric fish"—as the fish of these two groups have been designated—a leading model system in neurobiology for studies of how animals process sense data.

The principle of biological active electrolocation is that objects that differ in impedance from the surrounding medium distort a self-generated field, and an array of sensors ("electroreceptors") on the body detect these distortions. In prior work, we have provided evidence that changes as small as 0.1% of the baseline voltage across the skin (about one microvolt given the typical millivolt baseline) may be sensed by one species of weakly electric fish to guide a strike at small prey ($\sim$2 mm) at distances of up to $\sim$30 mm (about one quarter of a body length) [11], [14].

The work presented here has two motivations, one from basic science and the second from engineering. In this work we develop an approach for processing electrosensory data to control the position of an artificial electric field emitter and sensor array to localize objects. This is done without regard to mechanisms of biological active electrolocation, beyond the constraints of utilizing an applied field and voltage sensors. Our basic science motivation is to utilize our findings for comparison to knowledge gained through our ongoing investigations into biological electrolocation [14], [16], [11]. We expect this will yield helpful new avenues of research and experimentation. Our engineering motivation is that while current aerial and aquatic vehicles excel at high speed, long distance movement through uncluttered spaces, the sensing, control, and mechanical technology needed for low speed, high maneuverability movement through cluttered spaces is very poorly developed, yet an area of growing need [9].

In the sensory domain, such future vehicles have some distinct desirable attributes. First, the provisioned sensors must work well at short range. Second, rather than being concentrated on one portion of the hull of the vehicle (e.g., cameras at the front of a remotely operated vehicle), the sensors should be distributed over the entire surface of the vehicle. This is required to support high maneuverability, possibly omnidirectional movement in tight spaces. Third, to more robustly control sensory acquisition in geometrically complex spaces, such sensors should generate the energy that they subsequently transduce, as with radar and sonar systems [15]. Since these properties pertain to the biological systems that inspire the present work—weakly electric fish sense at short range, typically less than one body length; sensors are scattered over the entire body to support multidirectional movement; and it is an active sensory system—active electrolocation may provide a useful sensing and movement approach for a future class of underwater vehicles.

A. Prior Work in Electric Field Sensing

There are a few examples of engineered electric field sensing systems. One of the earliest was the Theremin, a musical instrument that made its first public appearance in 1921 and measures the player's capacitance relative to a set

This work was supported by NSF grant IOB-0517683. J. Solberg and K. Lynch are with the Department of Mechanical Engineering, M. MacIver (maciver@northwestern.edu) is with the Department of Mechanical Engineering, Department of Biomedical Engineering, and Department of Neurobiology and Physiology, Northwestern University, Evanston IL USA.

of transmitter/reciever antennae to determine the pitch of the output tone [21]. The Theremin is the first device that could measure the position of an object (the body parts of the player in this case) by measuring changes of an emitted electro-magnetic field. A system has been recently developed by the MIT Media Lab that is able to extract the 3-D position of a user's hand using principles similar to the Theremin [19].

More closely related to the present work is a previous study that built an artificial electrosensory array to study the feasibility of using such a system in underwater robots [10], [9]. They were able to determine the distance of a submerged 10 mm diameter plastic sphere up to a distance of about 12 mm away from the sensor. Their distance estimation algorithm was based on the spatial distribution of the sensor measurements A related study built an artificial electrosensory system to investigate the possibility of using such a system for obstacle avoidance in underwater robots [4]. Their system could detect either a conducting or insulating sphere 25 mm in diameter at a range of 5 mm. In their preliminary experiments the robot could perform obstacle avoidance using this electrosensory system.

B. Paper Overview

The next section describes a simple model that is able to predict the observed perturbation in an electric field due to a spherical target. It will be shown that simulations using this model are qualitatively similar to the empirical results examined in later sections. Section III describes the electrolocation system hardware and the method of constructing a probabilistic sensor model of a single object (the "electric image" of the object). The method for locating objects using electrosensory information are detailed in Section IV. Section V details the experimental facilities and protocol, and Section VI summarizes the results and implications of the electrolocation experiments.

II. Idealized Electrolocation

When an electric field is present around an object, the field induces a dipole at the object. The magnitude of the dipolar perturbation at a particular measurement point is a function of the object location, size, shape, and electrical contrast, as well as the electric field strength at the object. We will define the complete pattern of perturbations created by an object with a given applied field, along with the variance of those perturbations in the case of empirical measurements, as the "electric image" of the object. This pattern of perturbations is used by an active electrolocation system in identifying the position and properties of an object. The theoretical model used in this paper only considers spherical targets, and was derived by Rasnow in [17]:

$$\delta\phi(\mathbf{r}) = \frac{a^3 \mathbf{E}_\mathrm{f} \cdot \mathbf{r}}{|\mathbf{r}|^3} \left(\frac{\sigma_\mathrm{target} - \sigma_\mathrm{water}}{\sigma_\mathrm{target} + 2\sigma_\mathrm{water}} \right) \qquad (1)$$

where $\delta\phi(\mathbf{r})$ represents the change in potential (mV) at position $\mathbf{r}$ (cm) relative to the center of the target; a is the target's radius (cm); $\mathbf{E}_\mathrm{f}$ is the electric field vector at the location of the target (mV/cm); σ_target is the conductivity of the target, and σ_water is the conductivity of the water (μS/cm). The right term of Equation (1) within the parentheses is called the *electrical contrast factor* and denoted χ. The electrical contrast factor varies from $\chi = -1/2$ (for perfect insulators) to $\chi = +1$ (for perfect conductors). When the conductivity of the target and water are equal, the electrical contrast is zero and the target becomes electrically invisible. However, it should be noted that this model ignores phase shifts due to capacitive components of the target impedance. In weakly electric fish, such phase shifts are detected by a different electrosensory system [16]. Such phase shifts are likely used to differentiate between inanimate objects and live objects, which have capacitance due to biological membranes.

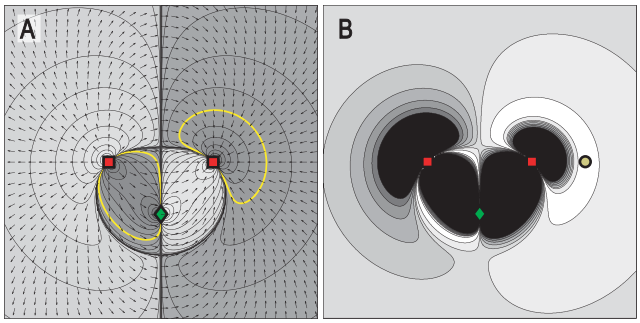

Fig. 1. (A) An idealized noiseless electric image of a perfectly conducting 1 cm diameter sphere. To compute this image, we place the sphere at each point on a grid covering the image. For each place on this grid, we compute the perturbation *at the green diamond (sensor)* according to Equation (1), given the field applied at the red squares. Intermediate values are interpolated. Arrows show the direction of the unperturbed electric field. Light gray designates positive perturbations of the simulated electric field as observed at the sensor, and dark gray designates negative perturbations of this field as observed at the sensor. The two yellow contours indicate the 1-D subspace to which the sphere located at any point on the contours can be localized after one measurement, if the electric image of this sphere is already known. (B) Probability distribution resulting from the 1 cm sphere being located at any position along the yellow contours (for example, at the position indicated by the filled yellow circle). Gaussian noise is added to the simulated sensor readings of (A). Each color represents a confidence interval (CI) based on the standard deviation of the probability mass of the PDF. White is the one-sigma CI, or 68.3%; white and the lightest gray together represent the two-sigma, or 95.5%, CI.

By applying this simple model we can gain some basic intuition into the challenges of active electrolocation. In Figure 1(A), we show the electric image of a 1 cm (diameter) spherical ideal conductor. An electric field is applied at the red squares, and a sensor (green diamond) measures the difference in voltage between the unperturbed and perturbed electric field. The black lines are perturbation isocontours. If we consider one perturbation value, such as the one indicated by the two yellow contours, a measurement of this value at the sensor can only show that the sphere is located somewhere on one of the two contours.

The isopotential perturbation contours of Figure 1(A) therefore represent the theoretical limit on how well a target of known properties can be localized by a single noiseless observation of the perturbation in 2-D. Each contour in Figure 1(A) represents the 1-D "localization subspace" of a target for the given sensor observation. It is impossible

to disambiguate the location of the 1 cm spherical ideal conductor from the location of any other 1 cm spherical ideal conductor (observed at a different time) located on the same contour. Real sensors, however, have noise. In this case, the contours become bands of probability according to the noise model for the sensor. For example, if the sphere is actually on one of the yellow contours in Figure 1(A)—such as at the position indicated by the filled yellow circle in Figure 1(B)—by assuming Gaussian noise of a certain mean and variance we can compute the probability distribution over the possible target locations. This probability distribution is shown in Figure 1(B). We discuss the algorithm for computing the probability distribution later in the paper.

III. Electrosensory Array and Field Emitter

Now that we have looked at idealized electrolocation in simulation, we describe the hardware and protocol behind our robotic active electrolocator.

A. Hardware

The electric field is generated by a 2 V (RMS) biphasic 1 kHz square wave. This electric field is transmitted between two silver electrodes submerged in water, which were plated with silver chloride to improve the metal-water electrical interface. The field emission electrodes are 51 mm apart. The two sensing electrodes are also 51 mm apart, arranged as shown in Figure 3(B). Both the electric field emission electrodes and the sensing electrodes are 0.38 mm diameter silver wires that are stabilized by 0.5 mm borate silicate glass pipettes (see [18] for more details on hardware for measuring electric fields). The two sensing electrodes are positioned to give identical readings with no object present. Perturbations are measured by amplifying the difference of the signals recorded at the two sensing electrodes with a high-gain differential amplifier.

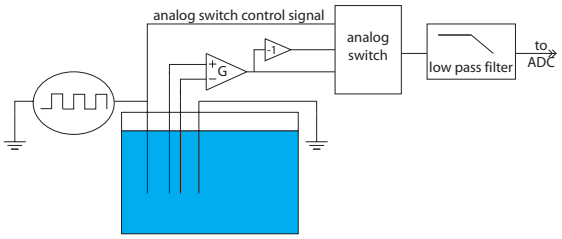

Fig. 2. **Schematic of the electrosensory circuit.**

After the sensor signals are differentially amplified, the resulting signal, along with its negative, is sent to an analog switch. The analog switch passes one of the two input signals to the output according to a switching signal, which is the original square wave used to generate the electric field. This serves as a matched filter, since only sensory signals of the same frequency as the field signal have a nonzero time-averaged mean at the output of the analog switch. The final stage is a low-pass filter that outputs this mean value. The technique used here is similar to the "synchronous detection" approach of the Flying Fish [20].

B. Measuring the Electric Image

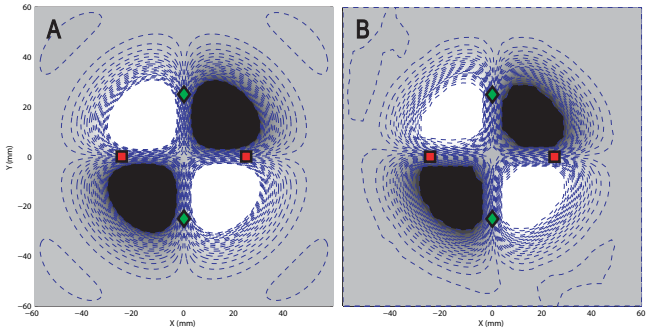

Fig. 3. **Theoretical and empirical electric images.** Red squares indicate the location of the electric field emission electrodes. Green diamonds indicate the location of the voltage sensing electrodes. The color map goes from white for +10 volts to gray for intermediate values to black for -10 volts. Dashed lines are at 500 mV increments. We only show the magnitude, not variance, component of the electric images. (A) Voltage perturbation versus position derived from Equation (1) using a perfectly conducting sphere 38.1 mm in diameter (contrast factor $\chi = +1$). This 2-D slice of modeled sensor voltages represents the horizontal plane (constant water depth) that is 3 mm above the top of the sphere. (B) Measured electric image with a 38.1 mm diameter stainless steel sphere just below the plane of the electrodes (about 3 mm) in low conductivity water (160 μS/cm). The color map for (A) was adjusted to saturate at the same voltages as our sensor circuit for comparison purposes. See Section V-C for more details on the measurement protocol.

The electric image of a spherical object can be estimated using Equation (1), as shown in Figure 3(A) Rather than estimate the image with the model, we measure the electric image by sampling the voltage at each point of a grid of locations (x_s, y_s), representing the location of the target in the sensor frame. By taking a number of readings at each grid point, the measured electric image consists of two grids of values: a grid of average sensor readings and a grid of sensor reading variance. The measurement of the sensor reading variance is a good estimate of the sensor uncertainty if the noise is Gaussian, which was approximately confirmed by our empirical data. Off-grid values are interpolated. The resulting mean and variance components of the electric image are denoted $\text{ave}(x_s, y_s)$ and $\text{var}(x_s, y_s)$, respectively, mapping the position of the target in the sensor frame to a sensor reading and variance. Figure 3(B) shows that the empirical electric image of a 38.1 mm diameter stainless steel sphere in low conductivity water is similar to the theoretical model constructed from Equation (1).

IV. Estimation and Control

An *active* target localization system requires a controller to prescribe subsequent sensor positions that will obtain useful information. We have chosen two control algorithms to compare their electrolocation effectiveness. One of these is a random walk, and thus is not active by the above definition. They both utilize a Monte Carlo-based control scheme that accounts for the stochastic nature of sensing and motion. They require that the electric image of the target be recorded prior to localization.

For both controllers belief about the position of the target is maintained via a particle filter. A particle filter tracks

a finite number of candidate target positions based on a forward simulation of their position (Monte Carlo simulation [12]). The particle filter is a type of Bayes filter, where beliefs are probabilistic and updated as new information comes in [22]. As illustrated in Figure 1(B), the belief in the location of the target may be ambiguous—with 95% confidence, the target is in one of the two white regions of the figure. One of the many applications of particle filters is localization and mapping in mobile robotics [5], [7], [22]. The robotic electrolocation problem is a variant of the localization problem, where the task is to determine the location of an external target as opposed to the location of the robot relative to some external coordinate frame. The particle filter algorithm consists of recursive implementations of both a predictive and a measurement update step, which are described below.

Predictive step. The predictive step integrates the control intention along with the motion model to estimate the next state. In most real-world scenarios the execution of the motion model increases the uncertainty of the belief. The XY robot used for these experiments has high-precision encoders and controllers to achieve accurate motion. Thus, the motion model introduced very little uncertainty into the belief about the target position. Thus, we did not employ a probabilistic motion model in our system. If motion uncertainty was significant, then techniques from SLAM (simultaneous localization and mapping) could be utilized to specifically compensate for these multiple sources of uncertainty. Alternatively, if only the relative location of the object is of interest, then the state space could be re-parameterized as the relative position between the robot and target.

Measurement update step. The measured electric image consists of the ave() and var() functions, as discussed in Section III-B. Given a cloud of M particles representing the current belief of the target location, then, a new sensor reading z_i assigns to each of those particles a weight according to how likely it is to explain the data. This weight is simply the value of a Gaussian at $(z_i - \text{ave}(x_s, y_s))/(\text{var}(x_s, y_s))^{1/2}$ standard deviations, where (x_s, y_s) is the location of the particle in the sensor frame. *Importance resampling* then selects particles M times randomly from a roulette wheel where each particle's slice of the wheel is proportional to its weight. This results in duplicate particles at the same location. To introduce diversity into the particle set, a small amount of normally-distributed noise (standard deviation of 1 mm) is then added to the position of each particle.

We choose a discrete-time formulation with a discrete set of 16 different control options. One of these is to remain stationary, and the other 15 are randomly sampled (new set at each time step) from the interior points of a square centered at the current robot position and with sides of length 20 mm. Thus, the robot can never move more than 10 mm in each dimension in a single time step. We tested two different policies for the probabilistic controller:

#1 **Random walk** (rnd wlk)
Randomly choose one of the possible control options.

#2 **Minimize expected variance of particles** (min var)
Choose the control option that minimizes the expected variance of the particles at the next step.

Controller **#2** uses greedy control laws, which attempt to maximize the expected information gain on the next step. Similar techniques have been successfully used in [2], [6], [13], where controllers minimize some scalar function of the covariance matrix (in the case of a Gaussian belief) or the entropy (in the case of nonparametric belief). Controller **#1** is essentially open-loop.

The *random walk* (**#1**) controller serves as the baseline to compare to the performance of the minimal variance controller. Controller **#2** (*minimize expected variance of particles*) utilizes *particle voting* (see Algorithm 1) to choose the control option. This method examines each particle and chooses the best control action under the assumption that the target is actually at that particle's location. Each particle can then be thought of as voting for a particular control action that works best for that particle. Once all of the votes are tallied, the control action with the most votes is chosen. Each particle's vote for the best control option is determined by evaluating the expected belief after executing each of the 16 control action and taking an observation. This observation is assumed to be the expected observation for this particular particle and control option combination. After each simulated control action and observation, the current particle cloud is resampled based on this simulated observation. The variance of this new (simulated) particle cloud serves as the metric for this control action. The control action that yields the lowest expected spatial variance of the particles receives the particle's vote.

Algorithm 1 Particle voting

for each particle, $m = 1$ to M, **do**
  Assume particle m is the true location of the target.
  for each control option, $c = 1$ to 16, **do**
    Simulate control option c and find the variance of the resultant particles based on the expected observation.
  end for
  Particle m votes for the control action that resulted in the lowest expected variance.
end for
The control option with the most votes is chosen.

V. Experimental Setup and Protocol

A. The Robot

The two sensing electrodes and the two electrodes that transmit the electric field are attached to a carriage above the tank. An XY table positions the carriage. The XY table consists of two orthogonal linear slides that are driven by DC motors. Two computers are used for information processing. One computer runs a real-time operating system (xPC, The

Mathworks, Natick MA USA) and handles low-level control of motors (PID position controller) and recording and filtering of the measurements. A second computer receives the filtered data from the real-time computer, generates the next position of the carriage, and sents it to the real-time computer. All algorithms were implemented with commercial numerical software (SIMULINK, Real Time Workshop, and MATLAB: The Mathworks, Natick MA USA).

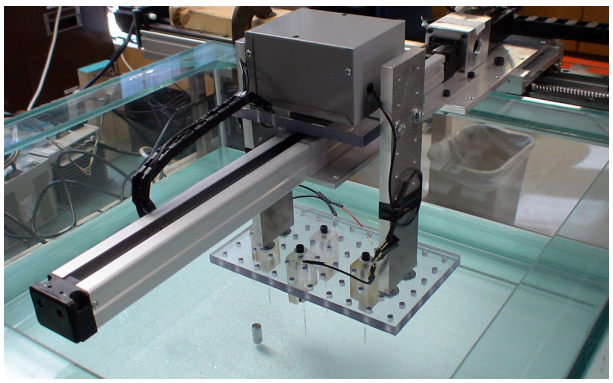

Fig. 4. **The electrolocation robot.** The Y linear slide is seen in the foreground and the X linear slide is in the background. A 24.5 mm diameter aluminum cylinder is in the tank of water. The electrodes are mounted to a translucent plastic breadboard.

B. Aquatic Environment

Experiments were conducted in a 750 mm by 750 mm glass tank filled to a depth of approximately 160 mm. In order to minimize the effects of the tank walls on the electric field, experiments were conducted in a central region of 200 mm by 200 mm. We used two different types of water, the first to mimic conductivity conditions in the natural habitat of weakly electric fish ("fresh") [11], [16], and the second to mimic ocean water conductivity. For each type of water sodium-chloride was added to de-ionized water until the desired salinity was obtained. The salinities of the two water types resulted in conductivities of 160 μS/cm for fresh water and $56,000$ μS/cm for marine water.

A small stand in the tank suspended the spherical targets such that the tops of the targets cleared the bottom of the electrodes. The electrical signature of the object stand alone did not significantly interfere with any of the measurements.

C. Object electric images

Electric images were recorded for each of the eight experimental conditions in Table I. For each target/water combination the target was placed at the center of the tank. For the 38.1 mm diameter spheres the robot moved the sensor carriage on a 120 mm by 120 mm grid, stopping every 4 mm to take a data point, for a total of $31 \times 31 = 961$ positions. For the 12.7 mm diameter spheres the robot moved the sensor carriage on a 80 mm by 80 mm grid, stopping every 4 mm to take a data point, for a total of $21 \times 21 = 441$ positions. The ave() and var() components were obtained by taking the average and variance of 10 time-averaged sensor readings at each grid point.

D. Active Electrolocation

Electrolocation was performed for the eight experimental conditions shown in Table I using both the controllers. For each condition both of the controllers started from 50 different positions for a total of 100 trials for each condition. Fifty starting positions were chosen randomly and this same set of 50 positions were used for both controllers. The target was always placed at the center (coordinates $\{x = 0, y = 0\}$) of the workspace. For the larger targets the robot was confined to start within coordinates $\{\pm 55, \pm 55\}$ and was permitted to move anywhere with coordinates of $\{\pm 60, \pm 60\}$. For the smaller targets the robot started at $\{\pm 40, \pm 40\}$ and stayed within $\{\pm 50, \pm 50\}$

Denoting the particle set covariance matrix as P, the robot keeps moving until $(\text{trace}(P))^{1/2} \leq 10$ mm (where $\text{trace}(P) = p_{xx} + p_{yy}$). If this stopping condition is not satisfied within 35 steps, the trial is labeled a failure. The elements of the covariance matrix are defined here as:

$$P = \begin{bmatrix} p_{xx} & p_{xy} \\ p_{yx} & p_{yy} \end{bmatrix}$$

VI. Experimental Results and Discussion

A. Electric images

Electric images were recorded for the eight different test conditions (Fig. 5). These give insight into the range and sensitivity of the electrolocation system for each of the target/water combinations. For example, the conditions under which the electric images in Figures 5(a) and 5(b) were made only differ in the conductivity of the target. Because metal has a high electrical conductivity, in fresh (low conductivity) water the object has high electrical contrast (Equation (1)). By comparison, Delrin plastic has low electrical conductivity; thus in fresh water this object has low contrast. Consequently, the magnitudes of the sensor readings are greater for the same relative robot positions. For the same level of noise between the two scenarios, the metal sphere can be detected further away than the plastic one.

While a high gain or large contrast factor favors longer range object detection, high gain can lead to adverse effects. Most of the electric images in Figure 5 exhibit significant regions that correspond to $+10$ V or -10 V due to saturation of the electronics. Referring back to the electric images in Figures 5(a) and 5(b), a sensor reading of $+10$ V would localize the target to within the two relatively large white lobes in Figure 5(a), but the sensor reading for the electric image in Figure 5(b) would localize the target to a much smaller region.

As the gain of the differential amplifier is increased, the amount of noise in the electronics downstream from the amplifier is also increased. Figures 5(e) and 5(f) have utilized an order of magnitude higher gain than the other electric image recordings. As a result, the images are noisier.

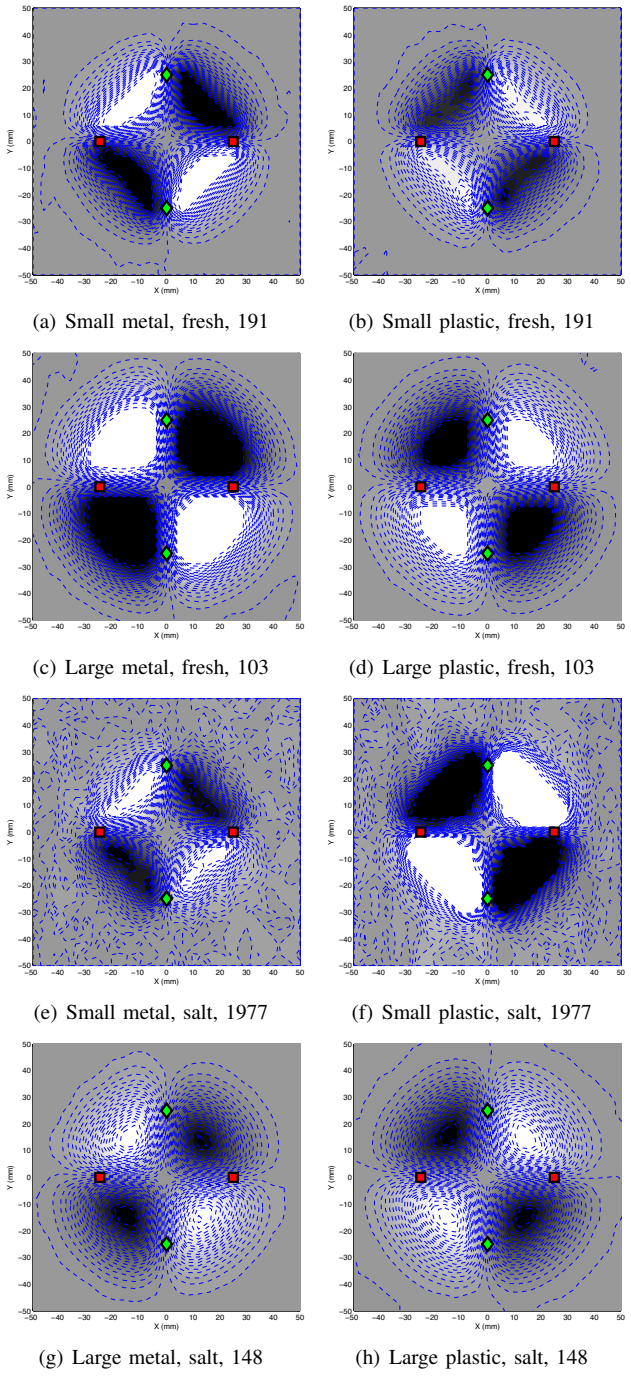

(a) Small metal, fresh, 191 (b) Small plastic, fresh, 191

(c) Large metal, fresh, 103 (d) Large plastic, fresh, 103

(e) Small metal, salt, 1977 (f) Small plastic, salt, 1977

(g) Large metal, salt, 148 (h) Large plastic, salt, 148

Fig. 5. **Electric images for the eight experimental conditions.** Caption legend: Small is a 12.7 mm diameter sphere, Large is a 38.1 mm diameter sphere, fresh is 160 μS/cm water, salt is 56,000 μS/cm water, and the last number is the differential amplifier gain. Metal is type 440-C stainless steel and plastic is Delrin plastic. Red squares indicate the location of the electric field dipoles. Green diamonds indicate the location of the voltage sensors. The color map goes from white for $+10$ volts to gray for intermediate values to black for -10 volts. Blue dashed lines are at 500 mV increments.

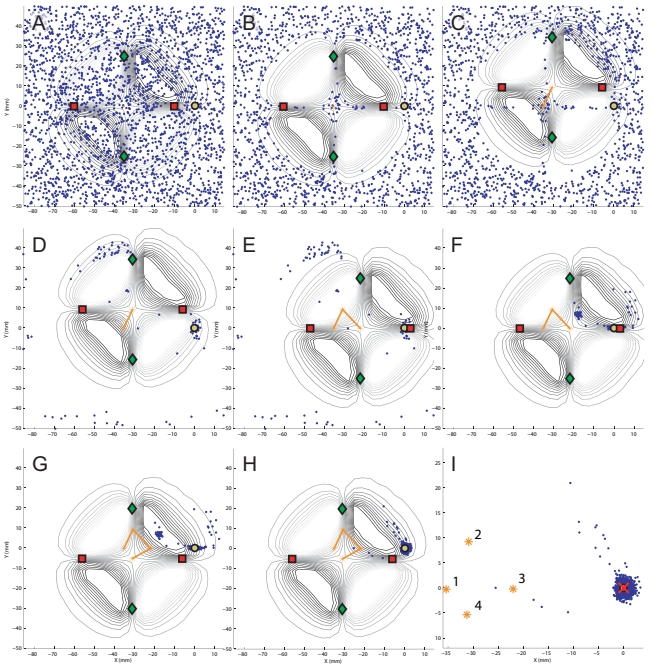

Fig. 6. **Snapshots of a typical electrolocation sequence.** The 2500 particles whose mean constitutes the estimate of the target position are shown as blue dots. The actual target location is a yellow circle, in this case the 12.7 mm diameter stainless steel sphere. The position of the electrodes on the robot are the green diamonds (sensors) and red squares (electric field emitter). The orange asterisks represent the path of the robot. The contours are iso-electric-field-perturbation gradations at approximately 1 V steps. The target is at coordinate $x = 0$, $y = 0$. (A) Initial belief; (B) First observation; (C) Move $\{+4.5, +9.5\}(mm)$; (D) Second observation; (E) Move $\{+8.9, -9.3\}$; (F) Third observation; (G) Move $\{-9.2, -5.1\}$; (H) Fourth observation; (I) The red "x" located at coordinate $x = 0.074$ and $y = 0.001$ is the centroid of the particles and is the final estimate of the location of the target. The numbered orange asterisks are the positions visited by the robot. Note that the axes have changed from the other subfigure.

B. Active Electrolocation

Electrolocation was performed using the electric images shown in Figure 5 for the targets shown in Table I. For a given starting position, if either controller yielded a failure trial, then data from these trials was omitted in calculating the mean error and the mean number of steps statistics. This was done because failure trials often resulted in errors much larger than successful trials. All data (included failure trials) were used in calculating the medians.

Table I shows the performance of the electrolocation controllers using three statistical measures:

1) **success trials:** This is the number of trials that were labeled a SUCCESS. The number next to it in parentheses is the number of trials that were labeled FAILURE.
2) **error:** This is the distance between the actual target location and the estimated target location at the end of the trials. The *mean* error only considers the trials that were a success for both controllers for that starting position, while the *median* error considers all trials.
3) **steps:** This is the number of steps needed to complete the trials. As described in the text, the mean calculation only considers successful trials while the median calculation accounts for all trials.

Figure 6 shows a typical electrolocation sequence. In Figure 6(B) the robot has updated its belief using a single observation and the particle filter algorithm described in

TABLE I

Electrolocation statistics for the eight experimental conditions tested for the particle filter-based control scheme. P=Plastic; S=Steel. Water salinity: fresh is 160 μS/cm; salt is $56,000$ μS/cm.

water salinity	sphere dia. [mm] / material	control type	success (failure)	error [mm] mean / median	# steps mean / median
fresh	12.7 / S	rnd wlk	41 (9)	2.0 / 1.5	10 / 9
fresh	12.7 / S	min var	50 (0)	1.7 / 1.1	10 / 5
fresh	12.7 / P	rnd wlk	35 (15)	2.1 / 2.0	9 / 10
fresh	12.7 / P	min var	50 (0)	1.5 / 1.1	10.0 / 6
fresh	38.1 / S	rnd wlk	32 (18)	2.2 / 2.8	15 / 23.5
fresh	38.1 / S	min var	44 (6)	1.4 / 1.5	9 / 6.5
fresh	38.1 / P	rnd wlk	35 (15)	2.4 / 2.8	10 / 9.5
fresh	38.1 / P	min var	49 (1)	2.2 / 2.4	9 / 5
salt	12.7 / S	rnd wlk	35 (15)	4.3 / 4.9	11 / 11
salt	12.7 / S	min var	49 (1)	3.9 / 3.7	10 / 7
salt	12.7 / P	rnd wlk	41 (9)	2.3 / 2.2	10 / 8.5
salt	12.7 / P	min var	50 (0)	2.7 / 1.9	7 / 5
salt	38.1 / S	rnd wlk	37 (13)	1.1 / 1.0	10 / 13
salt	38.1 / S	min var	45 (5)	1.3 / 1.0	11 / 6.5
salt	38.1 / P	rnd wlk	31 (19)	3.1 / 4.9	11 / 14.5
salt	38.1 / P	min var	44 (6)	2.9 / 2.8	11 / 12.5
all	conditions	rnd wlk	36 (14)	2.4 / 2.8	10.8 / 12.4
all	conditions	min var	48 (2)	2.2 / 1.9	9.7 / 6.7

IV. Since the sensor measurement is near the RMS noise assumed for the sensor, the particle filter kept most of the particles that correspond to a sensor reading of near 0 V. This trial uses the controller that minimizes the expected spatial variance of the particles at the next step. Based on the particles shown in Figure 6(B) the robot moves up 9.5 mm and right 4.5 mm. This "sense and move" sequence is repeated until the uncertainty is below the threshold (square root of the trace of the covariance is less than or equal to 10 mm). Figure 6(I) shows the final belief (blue dots).

A random walk (controller **#1**) was compared to controller **#2**, which minimized the expected variance of the particles (via particle voting) at the next step. Tables I and II summarize the statistics for the 800 target electrolocation trials and the 100 global localization trials (details on the global localization trials are described below). For both tasks the same algorithms were used, and for both controllers the statistics were computed in the same way. Table I also summarizes the overall performance of the two controllers in the last two rows.

If we examine the success trial statistics only, the mean error and the mean number of steps for completion do not make a compelling argument for choosing the minimum variance over the random walk controller. However, if we examine all trials including the failures, the median error and the median number of steps is significantly better for the active controller over the random walk.

TABLE II

Electrolocation statistics for the global localization experiment that the particle filter-based control scheme.

control type	success (failure)	Error [mm] mean / median	# steps mean / median
rnd wlk	48 (2)	1.3 / 1.0	11.8 / 11
min var	49 (1)	1.4 / 0.8	6.9 / 6

A particular trail is defined as a failure if it took more than 35 steps to localize the object or if the final error was greater than 15 mm. In almost all of the failure trials the robot took more than 35 steps to complete the task, which was a result of the robot getting lost. For the electrolocation of the 38.1 mm diameter plastic sphere in freshwater the random walk controller yielded 15 failures out of 50 possible trials (30% failure rate) while the active controller only had one (2% failure rate). As seen in figure 5(d), the electrosensory system would observe a reliable sensor measurement if the target was within roughly 45 mm of the center of the robot. But, for these trials the robot could start anywhere within $\{x = \pm 55, y = \pm 55\}$ from the location of the target. On average, the target fell within the 45 mm radius only about 53% of the time.

C. A Global Localization Scenario

Thus far we have utilized the active electrolocator to localize single spherical objects. The abilities of our electrosensory system extend past this specific task. From the standpoint of the particle filter-based electrolocation algorithm, it does not matter if the measured electric image is of a single target or of a complex layout of diverse objects.

For this set of experiments six cylinders of different diameters and conductivities were dispersed randomly with x and y coordinates within $\{x = \pm 80, y = \pm 80\}$. The goal of the robot was to localize itself relative to the origin of the map. Table II summarizes the performance of the global localization task for all 100 trials (50 trials for each controller).

VII. Conclusions

Weakly electric fish use a self-generated electric field and their population of 14,000 voltage-sensitive sensors to determine the spatial location of nearby objects. We have shown that our system, with one sensor, can successfully localize simple objects within water where the conductivity of both target and fluid were varied over a large range. First, we used an analytic model (Equation (1)) to develop an idealized (i.e., noise-free) electric image (Fig. 1(A)) and then discussed an example of a probabilistic belief based on a hypothetical noisy observation (Fig. 1(B)). A novel electrosensory system (Fig. 2 and Fig. 4) was presented

along with some electric images of simple objects it could record.

For the particle-filter-based electrolocation controller, the belief of the target took the form of a population of particles, where each particle represented a possible location of the target. As the robot received new measurements, the belief was updated via a particle filter. A greedy controller that minimized the expected variance of the particles was matched against a random walk (summary of results in Table I), and the same algorithms were applied to the global localization problem (summary of results in Table II). Our results show that our electrolocation system could usually locate the object within about 10 steps and with an average error of 2 to 3 mm across all the experimental conditions tested.

Several modifications could improve our current system. Future iterations of the electrosensory system could exploit time-varying gains of the differential amplifier. Armed with the controller's ability to dynamically change G, an electrolocation algorithm could take advantage of having both a high-gain electric image (good for long-range detection) and a lower-gain electric image (good for precise localization when near the object). Such an approach appears to be utilized in weakly electric fish [1]. Electrolocation algorithms could also be developed that do not require an empirical electric image *a priori*. Preliminary experiments have demonstrated an algorithm that uses specific features of electric images from a class of simple objects to determine their position. Alternatively, an electric image derived from a mathematical model, similar to that shown in Figure 3(A), could possibly be used if the required physical properties are known.

VIII. Acknowledgements

The authors would like to thank Michael Taylor for his efforts in getting the XY robot up and running. We would also like to thank Michael Peshkin for help with the sensor. The support of NSF grant IOB-0517683 is gratefully acknowledged.

References

[1] J. Bastian. Gain control in the electrosensory system mediated by descending inputs to the electrosensory lateral line lobe. *J. Neurosci.*, 6(2):553–562, 1986.

[2] F. Bourgault, A. A. Makarenko, S. Williams, B. Grocholsky, and H. Durrant-Whyte. Information based adaptive robotic exploration. In *IEEE/RSJ International Conference on Intelligent Robots and Systems (IROS 2002)*, Lausanne, Switzerland, 2002.

[3] T. H. Bullock and W. Heiligenberg, editors. *Electroreception*. Wiley, New York, 1986.

[4] G. Chetty and A. Russell. Electric field based obstacle avoidance. In *International Conference on Field and Service Robotics*, pages 378–382, Canberra, Australia, 1997.

[5] F. Dellaert, D. Fox, W. Burgard, and S. Thrun. Monte Carlo localization for mobile robots. In *Proceedings of the IEEE International Conference on Robotics and Automation*, 1999.

[6] D. Fox, W. Burgard, and S. Thrun. Active Markov localization for mobile robots. *Robotics and Autonomous Systems*, 25(3-4):195–207, 1998.

[7] D. Fox, S. Thrun, W. Burgard, and F. Dellaert. Particle filters for mobile robot localization. In A. Doucet, N. de Freitas, and N. Gordon, editors, *Sequential Monte Carlo Methods in Practice*. Springer-Verlag, New York, 2000.

[8] H. W. Lissmann and K. E. Machin. The mechanism of object location in *Gymnarchus niloticus* and similar fish. *J. Exp. Biol.*, 35:451–486, 1958.

[9] M. A. MacIver, E. Fontaine, and J. W. Burdick. Designing future underwater vehicles: principles and mechanisms of the weakly electric fish. *IEEE J Ocean Eng*, 29(3):651–659, 2004.

[10] M. A. MacIver and M. E. Nelson. Towards a biorobotic electrosensory system. *Autonomous Robots*, 11(3):263–266, 2001.

[11] M. A. MacIver, N. M. Sharabash, and M. E. Nelson. Prey-capture behavior in gymnotid electric fish: Motion analysis and effects of water conductivity. *J Exp Biol*, 204(3):543–557, 2001.

[12] N. Metropolis and S. Ulam. The Monte Carlo method. *J Amer Stat Assoc*, 44:335–341, 1949.

[13] L. Mihaylova, T. Lefebvre, H. Bruyninckx, K. Gadeyne, and J. de Schutter. Active sensing for robotics - a survey. Technical report, Katholieke Universiteit Leuven, Department of Mechanical Engineering, 2003.

[14] M. E. Nelson and M. A. MacIver. Prey capture in the weakly electric fish *Apteronotus albifrons*: Sensory acquisition strategies and electrosensory consequences. *J Exp Biol*, 202(10):1195–1203, 1999.

[15] M. E. Nelson and M. A. MacIver. Sensory acquisition in active sensing systems. *J Comp Physiol A*, 192(6):573–586, 2006.

[16] M. E. Nelson, M. A. MacIver, and S. Coombs. Modeling electrosensory and mechanosensory images during the predatory behavior of weakly electric fish. *Brain Behav. Evol.*, 59(4):199–210, 2002.

[17] B. Rasnow. The effects of simple objects on the electric field of *Apteronotus*. *J. Comp. Physiol. A*, 178(3):397–411, 1996.

[18] B. Rasnow. Measuring and visualizing EOD fields. In *Communication in Fishes*. Science Publishers, Enfield, NH, USA, 2006.

[19] J. Smith, T. White, C. Dodge, J. Paradiso, N. Gershenfeld, and D. Allport. Electric field sensing for graphical interfaces. *Computer Graphics and Applications, IEEE*, 18(3):54–60, 1998.

[20] J. R. Smith. *Electric field imaging, PhD thesis*. PhD thesis, MIT, 1999.

[21] L. S. Theremin and O. Petrishev. The design of a musical instrument based on cathode relays. *Leonardo Music Journal*, 6:49–50, 1996.

[22] S. Thrun, D. Fox, W. Burgard, and F. Dellaert. Robust Monte Carlo localization for mobile robots. *Artificial Intelligence*, 128(1-2):99–141, 2001.

[23] R. W. Turner, L. Maler, and M. Burrows, editors. *Electroreception and electrocommunication*. Proc. Satellite Symposium 5th Int. Congress Neuroethology, Cambridge, UK, 1999.